

Preparation, characterization, and cellular uptake of resveratrol-loaded trimethyl chitosan nanoparticles

Jeong Bin Min¹ · Eun Suh Kim¹ · Ji-Soo Lee¹ · Hyeon Gyu Lee¹

Received: 23 July 2017 / Revised: 21 November 2017 / Accepted: 24 November 2017 / Published online: 13 December 2017
© The Korean Society of Food Science and Technology and Springer Science+Business Media B.V., part of Springer Nature 2017

Abstract The aim of the study was to encapsulate resveratrol (RV) in trimethyl chitosan (TMC) nanoparticles cross-linked with tripolyphosphate (TPP) and/or alginate to achieve controlled release and improved cellular uptake. TMC (degree of quaternization of 78%) was prepared by reacting purified chitosan with iodomethane. Three types of RV-loaded TMC nanoparticles were prepared: TMC–TPP (TP-NPs), TMC–alginate (TA-NPs), and TMC–alginate–TPP (TAP-NPs). TA-NPs and TAP-NPs showed lower particle size and encapsulation efficiency (EE), better distribution, and more sustained release than TP-NPs due to the high molecular weight and viscous property of alginate. Caco-2 cellular uptake of RV was improved by TMC nanoencapsulation, and TP-NPs showed the highest uptake due to its significantly higher EE. Compared with TAP-NPs, TA-NPs with higher positive surface charge showed higher cellular uptake. Moreover, Caco-2 cell growth-inhibiting activity of RV was significantly increased by TMC nanoencapsulation and TP-NPs showed the significantly highest activity with a good agreement with the permeability results.

Keywords Trimethyl chitosan · Nanoencapsulation · Controlled release · Cellular uptake · Cytotoxicity

Introduction

Resveratrol (3,5,4'-trihydroxy-stilbene, RV) is a naturally occurring phytoalexin polyphenolic compound from the stilbenes family, mainly found in grape skins and peanuts [1]. Previous studies have demonstrated the various beneficial effects of RV on human health, including its antioxidant [2], anti-platelet aggregation [3], anti-inflammatory [4], and anti-carcinogenic activities [5]. However, RV has poor water solubility, limiting its incorporation into aqueous food products such as beverages [6]. Moreover, RV is easily isomerized from its trans form to its cis form, the latter of which has lower anti-oxidant and anti-inflammatory activity under UV light, at high temperature, and in an alkaline environment [7]. These properties decrease its bioavailability after oral administration and limit its utilization as a bioactive material in the food industry. Therefore, strategies are needed to overcome the poor aqueous solubility and low chemical stability of RV [8].

Encapsulation refers to technologies enabling the entrapment of core materials within wall materials like polymers. By coating bioactive materials with wall materials, encapsulation techniques are recognized as one of the most promising strategies for protecting sensitive materials from degradation owing to oxidative conditions such as moisture, heat, and radiation [9, 10]. Recently, encapsulation within nano-sized particles have received increased attention [11]. Due to the increased surface area resulting from size reduction, nanoparticles have many advantages such as good aqueous solubility and dispersity, reactivity, and efficient absorption through the cell membrane [12]. Since encapsulation can protect the core materials and improve physicochemical characteristics, this approach has been also utilized in biodelivery systems to maintain the

✉ Hyeon Gyu Lee
hyeonlee@hanyang.ac.kr

¹ Department of Food and Nutrition, Hanyang University, 222, Wangsimni-ro, Seoungdong-gu, Seoul 04763, Republic of Korea

viability of bioactive materials during gastrointestinal digestion [13].

Chitosan (CS), the linear polymer of acetylamino-D-glucose, is a natural polysaccharide obtained from the deacetylation of chitin [14]. Since CS has been approved as GRAS (Generally Recognized As Safe), it is frequently used as a wall material in the nanoencapsulation of food ingredients [15]. The cationic amino group of CS can interact with negatively charged materials through ionic gelation, resulting in formation of gel particles [16]. CS nanoparticles have been applied to various bioactive materials such as insulin [17], catechin [18], and ascorbic acid [19] and have been reported to enhance their bioactivity, stability, and intestinal absorption. Moreover, due to their mucoadhesive properties and capacity to open the tight junction, CS nanoparticles have been reported to enhance the intestinal absorption and bioavailability of encapsulated materials [20].

After orally administrated nanoparticles are delivered to the intestine, nanoparticles adhere to and infiltrate the mucosal layer, after which they pass through epithelial cell membranes [21]. However, since permeation enhancement has been attributed to electrostatic interactions between positively charged CS molecules and negatively charged sites in the tight junction, CS nanoparticles only exert their permeation-enhancing effects in the acidic gastric environment, where the amino group of CS is protonated [22]. Therefore, CS nanoparticles have limited potential as an oral delivery system to specific sites of the intestine where bioactive materials are commonly metabolized. Trimethyl chitosan chloride (TMC), the partially quaternized derivative of CS, was synthesized to overcome this drawback [23]. TMC is characterized by high solubility over a broad pH range and shows good permeation-enhancing properties, even in a neutral environment [24]. Therefore, TMC nanoparticles can be expected to have better performance than CS nanoparticles in a neutral environment.

The purpose of this study was to improve the cellular absorption of RV by encapsulation within TMC nanoparticles. RV-loaded TMC nanoparticles were fabricated on the basis of ionic gelation between TMC and a negatively charged material, tripolyphosphate (TPP) or alginate. The effects of nanoparticle type on various particle characteristics including particle size, polydispersity index (PDI), zeta potential (ZP), encapsulation efficiency (EE), and *in vitro* release were investigated. Moreover, the absorption of RV-loaded TMC nanoparticles to Caco-2 cells and their ability to inhibit cell growth were evaluated.

Materials and methods

Materials

CS (MW 50–190 kDa, 24 cps, 93% deacetylated), TPP (pentabasic, practical, 90–95%), RV, and sodium iodide were purchased from Sigma-Aldrich Chemical Co. Ltd. (St. Louis, MO, USA). N-methyl-2-pyrrolidone and iodo-methane (methyl iodide) were purchased from Junsei Chemical Co. (Tokyo, Japan) and Yakuri Pure Chemical Co. (Tokyo, Japan), respectively. Alginate (MW 75–150 kDa, 250 cps at 25 °C) was obtained from Kanto Chemical Co. (Tokyo, Japan). The Caco-2 colon carcinoma cell line was obtained from the Korean Cell Line Bank (KCLB, Seoul, South Korea). Dulbecco's modified Eagle medium (DMEM), fetal bovine serum (FBS), Hanks' balanced salt solution (HBSS), 0.25% trypsin–EDTA, HEPES, non-essential amino acids (NEAA), and glucose solution were purchased from Gibco Life Technologies (Grand Island, NY, USA). Phosphate-buffered saline (PBS) and penicillin–streptomycin were purchased from Lonza (Walkersville, MD, USA). 3,4,5-Dimethylthiazol-2-yl-2,5-diphenyltetrazolium bromide (MTT) was purchased from Sigma-Aldrich Chemical Co. Ltd. All other chemicals and solvents were of reagent grade and HPLC grade, respectively.

Synthesis of TMC

CS (2.0 g) and sodium iodide (4.8 g) were dissolved in 11 mL sodium hydroxide solution (15%, w/v). Then, the resulting solution was mixed with 11.5 mL methyl iodide and 80 mL 1-methyl-2-pyrrolidone solution in a 60 °C water bath (WB-22, Daihan Scientific Co. Ltd., Seoul, Korea) for 90 min. The mixture was added to 100 mL ethanol and centrifuged (Optima TL ultracentrifuge, Beckman, Fullerton, CA, USA) at 4 °C, 10,000×g for 30 min to collect the precipitated N-methylchitosan iodide. N-methylchitosan was redispersed in 80 mL 1-methyl-2-pyrrolidone and heated at 60 °C to remove residual ethanol. The N-methylchitosan suspension was mixed with 4.8 g sodium iodide, 11 mL NaOH solution (15%, v/v), and 7.0 mL methyl iodide under stirring and was heated at 60 °C for 60 min. The resulting suspension was mixed with 1.0 mL methyl iodide and 0.6 g NaOH under stirring for 60 min, after which 40 mL NaCl solution (10%, v/v) was added in order to substitute the iodide. Finally, the suspension was centrifuged (4 °C, 10,000×g, 30 min) after adding it to 100 mL ethanol. The precipitated TMC was lyophilized (TFD 5505, Ilsin Lab Co., Ltd, Seoul, Korea) into powder form [25].

H-NMR

¹H NMR spectra were collected on a Nuclear Magnetic Resonance Spectrometer (Bruker AVANCE 500 MHz, Bruker, Bremen, Germany). Briefly, TMC dissolved in D₂O (2 mg/mL) was introduced into a 5-mm NMR tube. The structural properties and degree of methylation of TMC are presented with the degree of quaternization (DQ), which was determined from the peak areas of the trimethylated amino acid and methyl groups using the equation below [26]:

$$DQ(\%) = [(fTMC)/(fH) \times 1/9] \times 100 \quad (1)$$

where *f*TMC and *f*H are the peak areas of the trimethyl amino acid (3.3 ppm) and methyl (4.7 and 5.7 ppm) groups, respectively. The 1H peak in the chitosan glucopyranose ring was used as a Ref. [27].

RV-loaded TMC nanoparticles

RV-loaded TMC nanoparticles were prepared by ionic gelation of TMC with negatively charged TPP and/or alginate [28]. Three types of nanoparticles were prepared with different wall material compositions (Table 1): TMC and TPP (TP-NPs); TMC and alginate (TA-NPs); and TMC, alginate, and TPP (TAP-NPs). Briefly, RV (0.05 mg/mL) was added to TMC aqueous solution (1.5 mg/mL) under stirring. Next, a TPP, alginate, or TPP and alginate mixed solution was added dropwise into the resulting solution using a peristaltic pump at 1 mL/min (Masterflex 7520-57; Cole Parmer Inc., Vernon Hills, IL, USA). The resultant nanoparticle suspensions were immediately

investigated for particles size, ZP, and PDI of the nanoparticles using a Zetasizer Nano-ZS instrument (Malvern Instruments Ltd., Worcestershire, UK).

Encapsulation efficiency

RV-loaded nanoparticles were centrifuged at 15,000×*g* for 30 min at 4 °C. The UV absorbance of the resulting supernatant at 306 nm was measured with a UV spectrophotometer (Thermo Scientific, Madison, WI, USA). The RV EE of the nanoparticles was determined as follows [29]:

$$EE(\%) = \frac{(\text{total amount RV} - \text{free amount RV in supernatant})}{\text{total amount RV}} \times 100 \quad (2)$$

In vitro release properties

The in vitro RV release properties of the nanoparticles were determined at pH of 3, 5, and 7 at 37 °C. After centrifuging as described above, the precipitated RV-loaded nanoparticles were redispersed in ethanol (2%, v/v), after which the pH was adjusted to 3, 5, or 7 with 0.1N HCl or NaOH solution. The nanoparticle suspensions were collected at different time-points and centrifuged at 15,000×*g* for 30 min at 4 °C. The concentration of released RV in the supernatant was determined with a UV spectrophotometer as described above. The RV release ratio was determined as follows [30]:

Table 1 Particle properties and encapsulation efficiencies of TMC nanoparticles with different tripolyphosphate and alginate concentrations

Type	Core material Resveratrol (mg/mL)	Wall materials			Particle size (nm)	Polydispersity index	Zeta potential (mV)	Encapsulation efficiency (%)
		TMC ¹ (mg/mL)	TPP ² (mg/ mL)	Alginate (mg/mL)				
TP-NPs	0.05	1.5	0.6	–	407.4 ± 59.3 ^b	0.667 ± 0.09	2.0 ± 0.3	71.9 ± 2.2 ^a
TA-NPs-10	0.05	1.5	–	0.15	310.6 ± 29.6 ^c	0.301 ± 0.06	35.5 ± 7.7	45.8 ± 12.4 ^b
TA-NPs-50	0.05	1.5	–	0.75	389.5 ± 52.7 ^{bc}	0.282 ± 0.02	18.7 ± 0.3	51.2 ± 11.23 ^b
TAP-NPs-10	0.05	1.5	0.6	0.15	346.7 ± 42.8 ^{bc}	0.380 ± 0.06	2.6 ± 0.1	47.5 ± 7.1 ^b
TAP-NPs-50	0.05	1.5	0.6	0.75	575.3 ± 56.9 ^a	0.339 ± 0.04	-44.2 ± 0.8	56.9 ± 2.7 ^b

^{a-c}Means in the same column with different letters are significantly different (*p* < 0.05)

¹trimethyl chitosan

²tripolyphosphate

$$\begin{aligned} & \text{Release ratio(\%)} \\ &= \frac{\text{amount of RV released from the nanoparticles}}{\text{amount of RV initially entrapped in the nanoparticles}} \\ & \quad \times 100 \end{aligned} \quad (3)$$

Cell culture

Caco-2 cells were cultured in DMEM (supplemented with 10% FBS, 5% NEAA, and 5% penicillin–streptomycin) at 37 °C. Cells were grown in an incubator with an environment of 5% CO₂ and 95% humidity, and the medium was changed every 2 days. All cells were used between passages 23 and 50 [31].

Confocal laser scanning microscopy

Qualitative Caco-2 cellular uptake of RV-loaded nanoparticles was investigated with a confocal laser scanning microscope (TCS SP5 AOBS, Leica, Mannheim, Germany) [32]. Caco-2 cells were seeded at a density of 4×10^5 cells/well on cover glasses in 6-well plates and then incubated for 24 h until reaching 50% confluence (JuLi Br live cell analyzer, NanoEnTek Inc, Seoul, South Korea). Next, RV and the nanoparticles were added to each well and incubated for 2 h. After aspiration of the medium, the cells were washed twice with PBS and incubated with 2% paraformaldehyde for 10 min at room temperature. The cells were washed thrice with PBS, after which the fluorescence of the RV-loaded nanoparticles was examined using a confocal microscope (excitation 480 nm/emission 405 nm). Fluorescence intensity was measured using Image J program (1.50i, National Institute of Health, USA).

Flow cytometry

The cellular uptake of the RV-loaded nanoparticles was quantified using a fluorescence-activated cell sorter (FACS Vantage SE, Becton–Dickinson, San Jose, CA, USA) [33]. Caco-2 cells were plated at a density of 4×10^5 cells/well in 6-well plates and cultured until reaching 70% confluence. RV and RV-loaded nanoparticles were added to each well, after which the mixtures were incubated for 1 h. After removing the medium, the cells were washed once with PBS and then detached by treatment with 0.5 mL of 0.25% trypsin. The cells were collected by centrifugation at 1500 rpm for 5 min and incubated with 2% paraformaldehyde for 10 min at room temperature. Next, the cells were washed twice with PBS and resuspended in 1 mL of PBS for flow cytometric analysis. Data from 10,000 events per sample were collected and analyzed

using Summit 5.1 software (BD Biosciences). All experiments were performed in triplicate.

Cytotoxicity

The cytotoxicity of the RV-loaded nanoparticles was evaluated using the MTT assay [34]. Briefly, Caco-2 cells were seeded at a density of 1×10^4 cells/well in a 96-well plate and incubated for 24 h. Next, the cells were incubated for an additional 72 h with 20 uL RV or RV-loaded nanoparticles, after which 20 uL of 0.5 mg/mL MTT in PBS was added to each well. After a 4 h incubation, the plate was centrifuged at 1500 rpm for 5 min, and the supernatants were removed. Formazan crystals were dissolved in each well by incubating the cells with 150 uL of dimethyl sulfoxide for 15 min at room temperature. The amount of formazan was measured using an ELISA microplate reader (ELx800UV, Bio-Tek Instrument Inc., Windoski, VT, USA) at 540 nm. The inhibition rate was determined as follows [27]:

$$\begin{aligned} & \text{Inhibition rate(\%)} \\ &= \frac{\text{Control absorbance} - \text{Experimental absorbance}}{\text{Control absorbance}} \times 100 \end{aligned} \quad (4)$$

Statistical analysis

All data are expressed as mean \pm standard deviation of three independent samples. Data were evaluated using one-way ANOVA followed by Duncan's multiple range test (SPSS Version 21.0, SPSS Inc., Chicago, IL, USA). P-values under 0.05 were considered statistically significant.

Results and discussion

Synthesis and characterization of TMC

Chitosan was methylated with CH₃I to yield TMC (Fig. 1). NMR analysis detected peaks at 2.8 and 3.3 ppm, which represented demethylation and trimethylation replacement of the methyl group hydrogen atom, respectively [35]. Moreover, the peak ranging from 4.5 to 5.5 ppm represented an anomeric hydrogen atom linked to the carbon atom at position 1 of the glucopyranose ring. The synthesized TMC showed a DQ of 78% in this study, which is similar to that of a previous study [36].

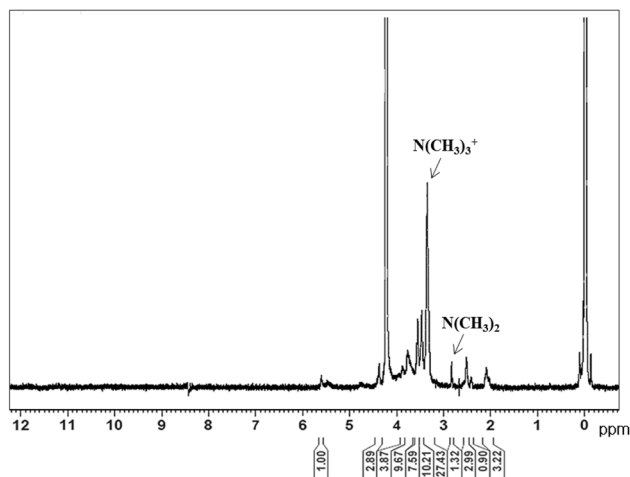


Fig. 1 $^1\text{H-NMR}$ spectrum of trimethyl chitosan

Characterization of RV-loaded TMC nanoparticles

RV-loaded nanoparticles were prepared by ionic crosslinking of the cationic TMC with anionic TPP or alginate (Table 1). When TMC is dissolved in aqueous phase, the amino groups undergo protonation. These positively charged amino groups are able to form gel particles by electrical attraction with TPP which is negatively charged in aqueous phase [19]. The optimal concentrations of TPP (0.6 mg/mL) and alginate (0.06 or 0.3 mg/mL) for nanoparticle formation were predetermined in preliminary experiments using fixed concentrations of TMC (1.5 mg/mL) and RV (0.5 mg/mL). The TP-NPs had a mean particle size of 407.4 ± 59.3 nm, with a PDI value of 0.667 ± 0.09 . Moreover, TA-NPs and TAP-NPs prepared with alginate were ranged from 310.6 to 389.5 nm and from 346.7 to 575.3 nm, respectively with a PDI values of approximately 0.3 (0.282–0.380). PDI is an important factor that indicates size distribution; values higher than 0.6 are regarded to indicate polydispersity, while values under 0.3 are considered to indicate monodispersity [37]. Therefore, the PDI of the TP-NPs indicates that size of these nanoparticles were not distributed uniformly in suspension while TA-NPs and TAP-NPs showed a homogeneous distribution. The physicochemical properties of nanoparticles prepared by ionic gelation between two oppositely charged materials have been reported to be influenced by the proportion of charged groups. Moreover, in previous studies, CS nanoparticles with small particle sizes and narrow size distributions tended to form at the optimal proportion of CS and cross-linker [38]. Thus, alginate seems to interact more effectively with a constant concentration of TMC (1.5 mg/mL) compared with the 0.6 mg/mL TPP used in this study from the results of lower particle sizes and PDI values of TA-NPs and TAP-NPs. The ZP of the TA-NPs and TAP-NPs decreased from

positive to negative values (from 35.5 to -44.2 mV) as the total concentrations of negatively charged TPP and alginate increased. Increased absolute ZP values have been reported to prevent particle coalescence and to improve nanoparticle stability due to the inter-particle repulsive forces [39]. Therefore, TA-NPs and TAP NPs are predicted to maintain a stable state over a longer period of time compared with TP-NPs.

Encapsulation efficiency

The RV EE of TP-NPs was $71.9 \pm 2.2\%$, while TA-NPs and TAP-NPs showed significantly lower efficiencies (Table 1). Moreover, EE was significantly increased from 45.8 to 51.2% and from 47.5 to 56.9% in both TA-NPs and TAP-NPs, respectively as the alginate concentration increased. EE has been reported to be affected by various factors; this result can be explained in terms of polymer molecular weight [40]. Alginate, a linear polysaccharide copolymer that consists of two sterically different repeating units, (1 \rightarrow 4)- α -L-glucuronic and (1 \rightarrow 4)- β -D-manuronic acid, in an irregular pattern forms a viscous solution when dissolved in aqueous solution. This high molecular weight biopolymer can form a gel by intermolecular interactions in presence of oppositely charged polymer, and has been used to reinforce the cohesion of porous particle structures. Therefore, the TA-NPs and TAP-NPs formed denser networks due to the presence of alginate and the decrease in internal space where RV is encapsulated. These effects resulted in significantly lower EE than for the TP-NPs. Alginate concentration did not have a significant effect on the EE of TA-NPs or TAP-NPs in this study.

In vitro release properties of RV-loaded TMC nanoparticles

Next, in vitro nanoparticle release of RV was studied in media at different pH at 37 °C (Fig. 2). All types of TMC nanoparticles released an initial burst of RV within the first hour, after which the release rate plateaued until the end of the incubation. The RV release rate also depended on the pH of dissolution media. As shown in Fig. 2A, the RV release rates from TP-NPs at pH 3 (24.15–25.15%) were higher than those at pH values above 3 (13.30–19.71%). TMC nanoparticles in this study were prepared by ionic gelation between different charged TMC and the other wall materials in the dissolved state. Thus, when the pH condition of the solvent is changed from suitable level, the ionic state of the wall materials could be changed, resulting in reducing of gel nanoparticles formation [41, 42]. Moreover, core materials encapsulated in nanoparticles can be released during physicochemical degradation of the particle structure. Therefore, one explanation for these

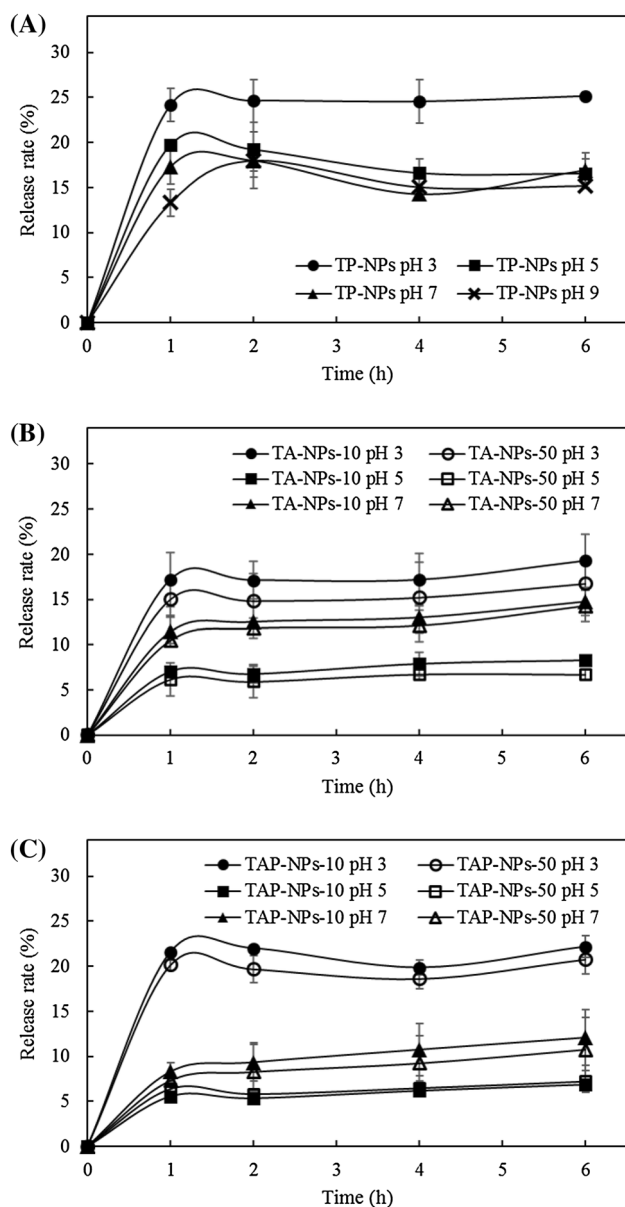


Fig. 2 *In vitro* fractional release rates of (A) TP-NPs, (B) TA-NPs, and (C) TAP-NPs in different pH environments at 37 °C. All data are the mean of three replicates and the error bars indicate the standard deviation

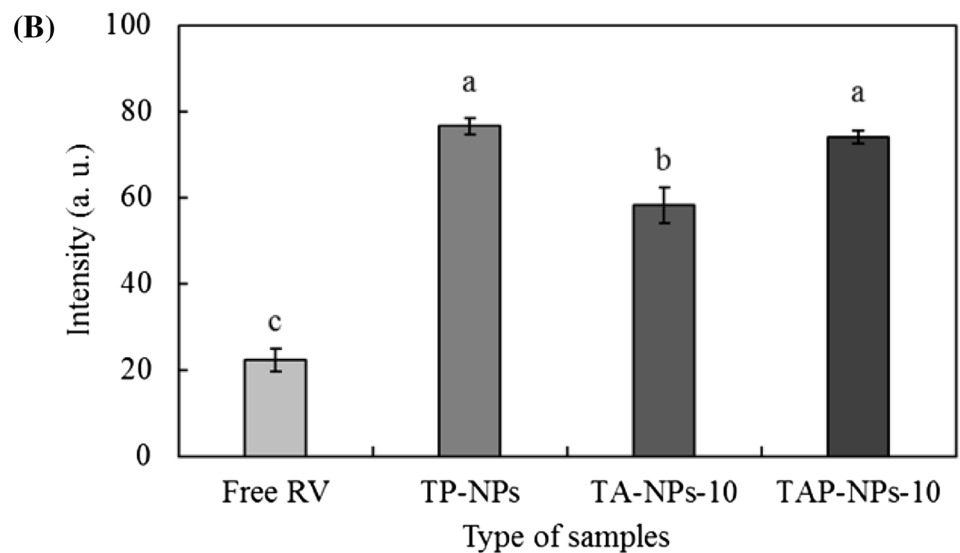
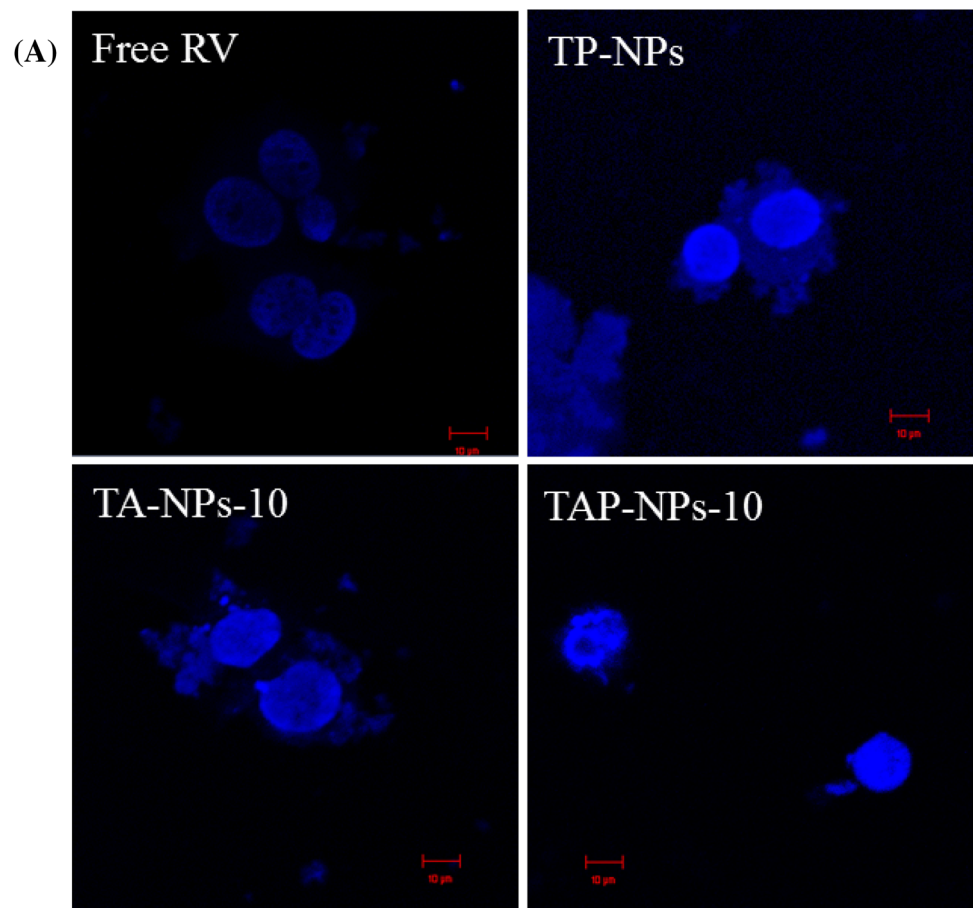
results is that CS polymers tend to swell in acidic environments due to protonation of the CS amino group. Thus, encapsulated RV could easily diffuse out of the nanoparticles into the dissolution media. On the other hand, structural degradation of CS nanoparticle was prevented by increasing the pH due to the lack of amino group protonation, resulting in prolonged RV release [43]. However, TP-NPs still have limitations in being effective oral delivery system because of its higher RV release rate at neutral pH similar to the intestinal environment where bioactive materials are commonly metabolized. TA-NPs

and TAP-NPs generally showed lower RV release rates compared with TP-NPs at the same incubation conditions (Fig. 2B, C). As mentioned above, alginate has been used to reinforce the cohesion of porous particle structures due to its viscous characteristic, thereby TMC nanoparticles prepared using alginate showed generally sustained RV release. TA-NPs and TAP-NPs showed the highest RV release rate at pH 3, followed by pH 7 and pH 5. Alginate gel showed an opposite trend compared with CS. Specifically, alginate gel is insoluble at acidic pH, while it is soluble in neutral and weakly basic solutions. Therefore, in the presence of alginate, the CS-alginate polyelectrolyte complexes of TA-NP and TAP-NP maintained a relatively stable state compared to the TMC-TPP complexes at low pH, thereby inhibiting RV release. On the other hand, since alginate is soluble and swells at neutral pH, release of RV from the slightly deformed TA-NPs and TAP-NPs was accelerated at pH 7 [44]. This finding, which is attributable to alginate, was more prominent for TA-NPs, which are produced by electrostatic interactions between only alginate and chitosan. In contrast, TAP-NPs, which are prepared with TPP and alginate, showed characteristics more similar to those of TP-NPs. In conclusion, TA and TAP-NPs also exhibited the release behavior in which the RV release was suppressed in gastric and promoted in intestinal environments. However, the use of alginate for the preparation of TMC nanoparticles appears to be a potential regulator of the gastrointestinal release of bioactive materials, and further studies are required.

Cell permeability

Intracellular uptake of free RV and of RV-loaded TMC nanoparticles was analyzed by confocal microscopy through visualization of the intrinsic blue fluorescence of RV (Fig. 3). Emission intensity was measured at wavelengths ranging from 400 to 722 nm at an excitation wavelength of 405 nm, and an emission wavelength of 480 nm, where a single absorption band was observed were selected for RV detection. Analysis of confocal images revealed that RV encapsulated within all types of TMC-nanoparticles was efficiently internalized after 1 h of incubation with Caco-2 cells. In the comparison according to the type of nanoparticles, TP-NPs (76.6 ± 1.9) and TAP-NPs (74.1 ± 1.6) showed significantly higher uptake rate compared with TA-NPs (58.2 ± 4.2). In contrast, only low fluorescence was observed in cells incubated with free RV (22.3 ± 2.5). One explanation for this result is that CS nanoparticles have been reported to enhance penetration of phenolic compounds across the intestinal epithelium by a paracellular or transcellular pathway, presumably because CS can control disruption of tight junctions along the epithelial cell barrier [45].

Fig. 3 Fluorescence (A) images and (B) intensity of Caco-2 cells treated with free resveratrol (0.5 mg/mL), TP-NPs, TA-NPs-10, and TAP-NPs-10 by confocal microscopy



The effect of TMC nanoparticle types on RV intracellular uptake was confirmed by flow cytometry, where the shift of peak fluorescence intensity to the right along the X axis reveals the degree of bioactive material internalization (Fig. 4). After 1 h of incubation, all of the peak of RV encapsulated in TMC-NPs shifted to the right along the X

axis compared with the peak of free RV. Moreover, the peak of RV encapsulated in TP-NPs showed the greatest movement width, followed by TA-NPs-10 and then TAP-NPs-10. This result can be interpreted primarily in terms of EE (Table 1). Transportation of phenolic material across intestinal epithelial cells is governed by passive diffusion,

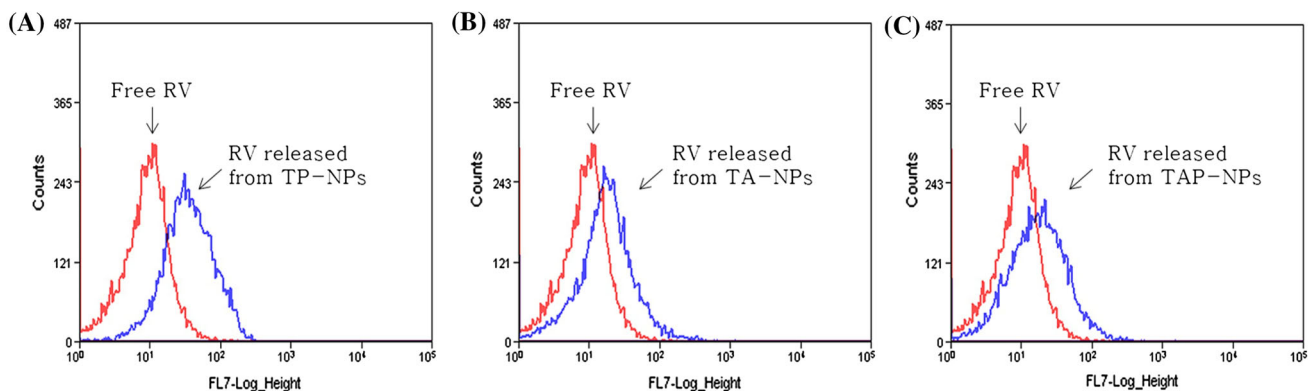


Fig. 4 Flow cytometry of (A) TP-NPs, (B) TA-NPs-10, and (C) TAP-NPs-10. The x-axis shows red (RV) and blue (RV-loaded TMC nanoparticles) fluorescence intensity, and the y-axis shows the

number of events recorded for a corresponding fluorescence intensity. (Color figure online)

including both paracellular and transcellular diffusion. Moreover, it has been reported that cellular uptake of RV is increased in a dose-dependent manner in both passive diffusion mechanisms [46]. Therefore, the finding that RV was encapsulated significantly more efficiently within TP-NPs compared with the other TMC nanoparticles could explain why the TP-NPs showed higher RV uptake than the TA-NPs-10 and TAP-NPs-10, since the TP-NPs contained more RV. On the other hand, compared with TAP-NPs-10, TA-NPs-10 showed higher positive ZP, even though the EE of the two nanoparticle types were significantly similar (Table 1). The cellular uptake of nanoparticles is influenced by various factors, among which interactions between nanoparticles and the cell surface are the most important [47]. Since the cell surface is negatively charged, highly positively charged nanoparticles adhere much more strongly to the cell surface [48]. Therefore, TA-NPs-10, which had significantly higher positive charges and ZP, could show better cellular uptake compared with neutral TAP-NPs-10 [49]. Consequently, though the RV release behavior of the TNC nanoparticles have partially limitation for gastrointestinal delivery, TMC nanoencapsulation could be effective for improving cellular uptake of RV.

Cytotoxicity

The viability of Caco-2 cells was decreased after treatment with RV (Fig. 5). Moreover, growth inhibition was significantly increased as the RV concentration increased from 0.5 to 1.5 mg/mL. The growth-inhibiting activity of RV was significantly increased by TMC nanoencapsulation compared with the same concentration of RV (0.5 mg/mL) or even compared with higher concentrations (1.0 to 1.5 mg/mL). Moreover, depending on the TMC nanoparticle type, TP-NPs showed significantly higher growth-inhibiting activity than TA-NPs or TAP-NPs. Since the

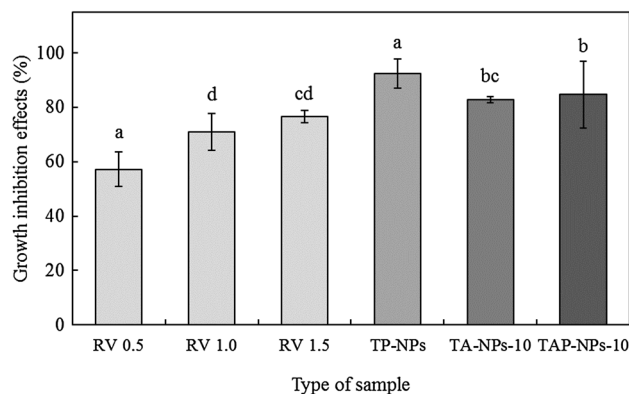


Fig. 5 Resveratrol-mediated inhibition of TP-NPs, TA-NPs-10, and TAP-NPs-10 on Caco-2 cancer cell growth. All data are the mean of three replicates and the error bars indicate the standard deviation. Different lowercase letters indicate significant differences ($p < 0.05$)

antitumor activity of RV against colon cancer cell lines is activated after cellular uptake, these results are in good agreement with the cellular uptake data that cellular uptake of RV was the most effective by encapsulation within TP-NPs.

In conclusion, RV was encapsulated within three types of TMC nanoparticles: TP-NPs, TA-NPs, and TAP NPs, respectively. TP-NPs was 407.4 ± 59.3 nm in size with lower ZP (2.0 ± 0.3 mV) and significantly higher EE ($71.9 \pm 2.2\%$) than the others. For RV-loaded TA-NPs and TAP-NPs, particle sizes were increased as alginate concentration increased, regardless of the presence of TPP. Moreover, RV EE (45.8 – 56.9%) decreased as alginate was added, but increased as alginate concentration increased from 10 to 50%. In in vitro release experiments, TMC nanoparticles showed higher sustained release and better release behavior as the substitution of alginate for TPP. Owing to the soluble characteristics of alginate, RV release was suppressed and accelerated at acidic and neutral pH, respectively. The results of confocal microscopy

and flow cytometry for RV cellular internalization evaluation showed that cellular uptake of RV was improved by TMC nanoencapsulation; specifically, uptake levels were increased at higher EE and ZP. In agreement with the cellular uptake results, RV-mediated growth inhibition was most greatly enhanced by TA-NPs, followed by TA-NPs and then TAP-NPs. These results suggest that RV-loaded nanoencapsulation using TMC is a good technique to improve the cellular uptake of RV. Moreover, although additional supporting research is necessary, it also suggests the possibility of alginate to achieve the effective controlled release of bioactive materials from CS nanoparticles.

Acknowledgements This research was supported by the Basic Science Research Program through the National Research Foundation of Korea (NRF), which is funded by the Ministry of Science, ICT, & Future Planning (No. 2014M3A7B4051898).

References

- Gresele P, Cerletti C, Guglielmini G, Pignatelli P, de Gaetano G, Violi F. Effects of resveratrol and other wine polyphenols on vascular function: an update. *J. Nutr. Biochem.* 22:201–211 (2011)
- Lekli I, Ray D, Das DK. Longevity nutrients resveratrol, wines and grapes. *Genes Nutr.* 5:55–60 (2010)
- Das S, Das DK. Resveratrol: a therapeutic promise for cardiovascular diseases. *Recent Pat. Cardiovasc. Drug Discov.* 2:133–138 (2007)
- Alarcon De La Lastra C, Villegas I. Resveratrol as an anti-inflammatory and anti-aging agent: Mechanisms and clinical implications. *Mol. Nutr. Food Res.* 49:405–430 (2005)
- Athar M, Back JH, Kopelovich L, Bickers DR, Kim AL. Multiple molecular targets of resveratrol: Anti-carcinogenic mechanisms. *Arch. Biochem. Biophys.* 486:95–102 (2009)
- Sessa M, Tsao R, Liu R, Ferrari G, Donsi F. Evaluation of the stability and antioxidant activity of nanoencapsulated resveratrol during in vitro digestion. *J. Agric. Food Chem.* 59:12352–12360 (2011)
- Zupančič Š, Lavrič Z, Kristl J. Stability and solubility of trans-resveratrol are strongly influenced by pH and temperature. *Eur. J. Pharm. Biopharm.* 93:196–204 (2015)
- Davidov-Pardo G, McClements DJ. Resveratrol encapsulation: designing delivery systems to overcome solubility, stability and bioavailability issues. *Trends Food Sci. Technol.* 38:88–103 (2014)
- Fang Z, Bhandari B. Encapsulation of polyphenols—a review. *Trends Food Sci. Technol.* 21:510–523 (2010)
- Shahidi F, Han XQ. Encapsulation of food ingredients. *Crit. Rev. Food Sci. Nutr.* 33:501–547 (1993)
- Ezhilarasi P, Karthik P, Chhanwal N, Anandharamakrishnan C. Nanoencapsulation techniques for food bioactive components: a review. *Food Bioproc. Tech.* 6:628–647 (2013)
- Esfanjani AF, Jafari SM. Biopolymer nano-particles and natural nano-carriers for nano-encapsulation of phenolic compounds. *Colloid Surf. B-Biointerfaces* 146:532–543 (2016)
- de Vos P, Faas MM, Spasojevic M, Sikkema J. Encapsulation for preservation of functionality and targeted delivery of bioactive food components. *Int. Dairy J.* 20:292–302 (2010)
- Kean T, Thanou M. Biodegradation, biodistribution and toxicity of chitosan. *Adv. Drug Deliv. Rev.* 62:3–11 (2010)
- Chaudhury A, Das S. Recent advancement of chitosan-based nanoparticles for oral controlled delivery of insulin and other therapeutic agents. *AAPS PharmSciTech* 12:10–20 (2011)
- Kim ES, Lee J-S, Lee HG. Nanoencapsulation of red ginseng extracts using chitosan with polyglutamic acid or fucoidan for improving antithrombotic activities. *J. Agric. Food Chem.* 64:4765–4771 (2016)
- Pan Y, Li Y-J, Zhao H-Y, Zheng J-M, Xu H, Wei G, Hao J-S. Bioadhesive polysaccharide in protein delivery system: chitosan nanoparticles improve the intestinal absorption of insulin in vivo. *Int. J. Pharm.* 249:139–147 (2002)
- Dube A, Nicolazzo JA, Larson I. Chitosan nanoparticles enhance the intestinal absorption of the green tea catechins (+)-catechin and (–)-epigallocatechin gallate. *Eur. J. Pharm. Sci.* 41:219–225 (2010)
- Jang K-I, Lee HG. Stability of chitosan nanoparticles for L-ascorbic acid during heat treatment in aqueous solution. *J. Agric. Food Chem.* 56:1936–1941 (2008)
- Vllasaliu D, Exposito-Harris R, Heras A, Casettari L, Garnett M, Illun L, Stolnik S. Tight junction modulation by chitosan nanoparticles: comparison with chitosan solution. *Int. J. Pharm.* 400:183–193 (2010)
- Ensign LM, Cone R, Hanes J. Oral drug delivery with polymeric nanoparticles: the gastrointestinal mucus barriers. *Adv. Drug Deliv. Rev.* 64:557–570 (2012)
- Lin Y-H, Mi F-L, Chen C-T, Chang W-C, Peng S-F, Liang H-F, Sung H-W. Preparation and characterization of nanoparticles shelled with chitosan for oral insulin delivery. *Biomacromolecules* 8:146–152 (2007)
- Sadeghi A, Dorkoosh F, Avadi M, Weinhold M, Bayat A, Delie F, Gurny R, Larijani B, Rafiee-Tehrani M, Junginger H. Permeation enhancer effect of chitosan and chitosan derivatives: comparison of formulations as soluble polymers and nanoparticulate systems on insulin absorption in Caco-2 cells. *Eur. J. Pharm. Biopharm.* 70:270–278 (2008)
- Chen F, Zhang Z-R, Yuan F, Qin X, Wang M, Huang Y. *In vitro* and *in vivo* study of N-trimethyl chitosan nanoparticles for oral protein delivery. *Int. J. Pharm.* 349:226–233 (2008)
- Cafaggi S, Russo E, Stefani R, Leardi R, Caviglioli G, Parodi B, Bignardi G, De Totero D, Aiello C, Viale M. Preparation and evaluation of nanoparticles made of chitosan or N-trimethyl chitosan and a cisplatin–alginate complex. *J. Control. Release* 121:110–123 (2007)
- Sieval A, Thanou M, Kotze A, Verhoef J, Brussee J, Junginger H. Preparation and NMR characterization of highly substituted N-trimethyl chitosan chloride. *Carbohydr. Polym.* 36:157–165 (1998)
- Jintapattanakit A, Mao S, Kissel T, Junyaprasert VB. Physicochemical properties and biocompatibility of N-trimethyl chitosan: effect of quaternization and dimethylation. *Eur. J. Pharm. Biopharm.* 70:563–571 (2008)
- Chen F, Zhang Z-R, Huang Y. Evaluation and modification of N-trimethyl chitosan chloride nanoparticles as protein carriers. *Int. J. Pharm.* 336:166–173 (2007)
- Koo SH, Lee J-S, Kim G-H, Lee HG. Preparation, characteristics, and stability of glutathione-loaded nanoparticles. *J. Agric. Food Chem.* 59:11264–11269 (2011)
- Sarmiento B, Ribeiro A, Veiga F, Sampaio P, Neufeld R, Ferreira D. Alginate/chitosan nanoparticles are effective for oral insulin delivery. *Pharm. Res.* 24:2198–2206 (2007)
- Jang K-I, Lee J-S, Lee HG. Physicochemical properties and cell permeation efficiency of l-ascorbic acid loaded nanoparticles prepared with N-trimethyl chitosan and N-triethyl chitosan. *Food Sci. Biotechnol.* 23:1867–1874 (2014)

32. Díaz TG, Merás ID, Rodríguez DA. Determination of resveratrol in wine by photochemically induced second-derivative fluorescence coupled with liquid–liquid extraction. *Anal. Bioanal. Chem.* 387:1999–2007 (2007)
33. Chakraborty PK, Mustafi SB, Raha S. Pro-survival effects of repetitive low-grade oxidative stress are inhibited by simultaneous exposure to resveratrol. *Pharmacol. Res.* 58:281–289 (2008)
34. Sergent T, Garsou S, Schaut A, De Saeger S, Pussemier L, Van Peteghem C, Larondelle Y, Schneider Y-J. Differential modulation of ochratoxin A absorption across Caco-2 cells by dietary polyphenols, used at realistic intestinal concentrations. *Toxicol. Lett.* 159:60–70 (2005)
35. Curti E, de Britto D, Campana-Filho SP. Methylation of chitosan with iodomethane: effect of reaction conditions on chemoselectivity and degree of substitution. *Macromol. Biosci.* 3:571–576 (2003)
36. Polnok A, Borchard G, Verhoef J, Sarisuta N, Junginger H. Influence of methylation process on the degree of quaternization of N-trimethyl chitosan chloride. *Eur. J. Pharm. Biopharm.* 57:77–83 (2004)
37. Gordon S, Teichmann E, Young K, Finnie K, Rades T, Hook S. *In vitro* and *in vivo* investigation of thermosensitive chitosan hydrogels containing silica nanoparticles for vaccine delivery. *Eur. J. Pharm. Sci.* 41:360–368 (2010)
38. Fan W, Yan W, Xu Z, Ni H. Formation mechanism of monodisperse, low molecular weight chitosan nanoparticles by ionic gelation technique. *Colloid Surf. B-Biointerfaces* 90:21–27 (2012)
39. Hu Y, Jiang X, Ding Y, Ge H, Yuan Y, Yang C. Synthesis and characterization of chitosan–poly (acrylic acid) nanoparticles. *Biomaterials* 23:3193–3201 (2002)
40. Wu Y, Yang W, Wang C, Hu J, Fu S. Chitosan nanoparticles as a novel delivery system for ammonium glycyrrhizinate. *Int. J. Pharm.* 295:235–245 (2005)
41. Huang G-Q, Xiao J-X, Jia L, Yang J. Complex coacervation of O-carboxymethylated chitosan and gum arabic. *Int. J. Polym. Mater. Po.* 64:198–204 (2015)
42. Butstraen C, Salaün F. Preparation of microcapsules by complex coacervation of gum Arabic and chitosan. *Carbohydr. Polym.* 99:608–616 (2014)
43. Anitha A, Deepagan V, Rani VD, Menon D, Nair S, Jayakumar R. Preparation, characterization, *in vitro* drug release and biological studies of curcumin loaded dextran sulphate–chitosan nanoparticles. *Carbohydr. Polym.* 84:1158–1164 (2011)
44. Shi X, Du Y, Sun L, Zhang B, Dou A. Polyelectrolyte complex beads composed of water-soluble chitosan/alginate: Characterization and their protein release behavior. *J. Appl. Polym. Sci.* 100:4614–4622 (2006)
45. Ranaldi G, Marigliano I, Vespignani I, Perozzi G, Sambuy Y. The effect of chitosan and other polycations on tight junction permeability in the human intestinal Caco-2 cell line. *J. Nutr. Biochem.* 13:157–167 (2002)
46. Zhao H, Yung LYL. Addition of TPGS to folate-conjugated polymer micelles for selective tumor targeting. *J. Biomed. Mater. Res. A* 91:505–518 (2009)
47. Xia T, Kovochich M, Liong M, Meng H, Kabehie S, George S, Zink JJ, Nel AE. Polyethyleneimine coating enhances the cellular uptake of mesoporous silica nanoparticles and allows safe delivery of siRNA and DNA constructs. *ACS nano* 3:3273–3286 (2009)
48. Cai Z, Wang Y, Zhu L-J, Liu Z-Q. Nanocarriers: a general strategy for enhancement of oral bioavailability of poorly absorbed or pre-systemically metabolized drugs. *Curr. Drug. Metab.* 11:197–207 (2010)
49. Yue Z-G, Wei W, Lv P-P, Yue H, Wang L-Y, Su Z-G, Ma G-H. Surface charge affects cellular uptake and intracellular trafficking of chitosan-based nanoparticles. *Biomacromolecules* 12:2440–2446 (2011)